Theor Chem Acc (2014) 133:1549
DOI 10.1007/s00214-014-1549-7

REGULAR ARTICLE

Mechanism and regioselectivity of the cycloaddition between nitrone and dirhodium vinylcarbene catalyzed by $Rh_2(O_2CH)_4$: a computational study

Xin Yang · Pan Xu · Ying Xue

Received: 24 May 2014 / Accepted: 16 July 2014 / Published online: 9 August 2014

Abstract The B3LYP density functional studies on the cycloaddition between nitrone and dirhodium vinylcarbene with subsequent cascade carbenoid aromatic cycloaddition/N–O cleavage and rearrangement revealed the energetics and the geometries of important intermediates and transition states in the catalytic cycle. The reaction initially occurs through a stepwise [3+2]-cycloaddition in which the dirhodium carbene activates the adjacent vinyl group for [3+2]-cycloaddition by the nitrone. Driven by the reactivity of the carbene carbon, intramolecular cyclopropanation takes place to release the catalyst, followed by the electrocyclic opening of the cyclopropane ring to form a seven-membered ring intermediate. N–O cleavage and [1,7]-oxygen migration to final product proceed in a single step with a high activation energy. With *meta*-substituent (Cl) in the *N*-aryl group, the charge density of chlorine's *ortho*-site decreases due to the negative inductive effect of chlorine. Therefore, as compared to the electrophilic addition on the C^8 atom, the electrophilic addition on the C^9 site owns a significantly incensement on the energy barrier of cyclopropane (**TSIII** and **TSIX**). In addition, according to the calculations, the basicity of the product **4** is stronger than that of the product **5**. So an acidic compound 1,1,1,3,3,3-hexafluoro-2-propanol added in the experimental study (Wang et al. in Angew Chem Int Ed 51:5907–5910, 2012) more easily reacts with **4** than **5** and thus promotes the formation of product **4**.

Keywords Dirhodium vinylcarbene · DFT calculation · Transition state · Reaction mechanism · Regioselectivity

1 Introduction

Diazo compounds have been extensively studied during the last few decades, and their value in organic synthesis is well known [1–5]. Transition-metal carbenoids derived from reactions of diazo compounds with a variety of metal complex are versatile intermediates in organic synthesis [6]. For several years, the rhodium-catalyzed reactions of donor/acceptor-substituted carbenoids have been explored, and the results showed that those carbenoids display much greater chemoselectivity when compared to the more conventional acceptor-substituted carbenoids [7–10]. A clear example of this effect is seen in a Hammett study of intermolecular cyclopropanation of *para*-substituted styrenes (Scheme 1) [11]. Electronic character of styrenes [ρ value of -0.9 (σ^+ scale)] can strongly affect the relative rates of reaction of methyl phenyldiazoacetate with various styrenes, while ethyl diazoacetate shows virtually no selectivity [11]. The greater chemoselectivity of the donor/acceptor carbenoids has opened up a number of reactions that were previously not viable with conventional carbenoids. In particular, vinylcarbene intermediates derived from vinyldiazoacetates exhibit a high level of selectivity in cyclopropanation [12–14] and carbon–hydrogen insertion reaction [15–17] and can participate in a diverse array of more elaborate transformation [15, 18, 19], such as the

Dedicated to Professor Guosen Yan and published as part of the special collection of articles celebrating his 85th birthday.

Electronic supplementary material The online version of this article (doi:10.1007/s00214-014-1549-7) contains supplementary material, which is available to authorized users.

X. Yang · P. Xu · Y. Xue (✉)
Key Laboratory of Green Chemistry and Technology in Ministry of Education, College of Chemistry, Sichuan University, Chengdu 610064, People's Republic of China
e-mail: yxue@scu.edu.cn

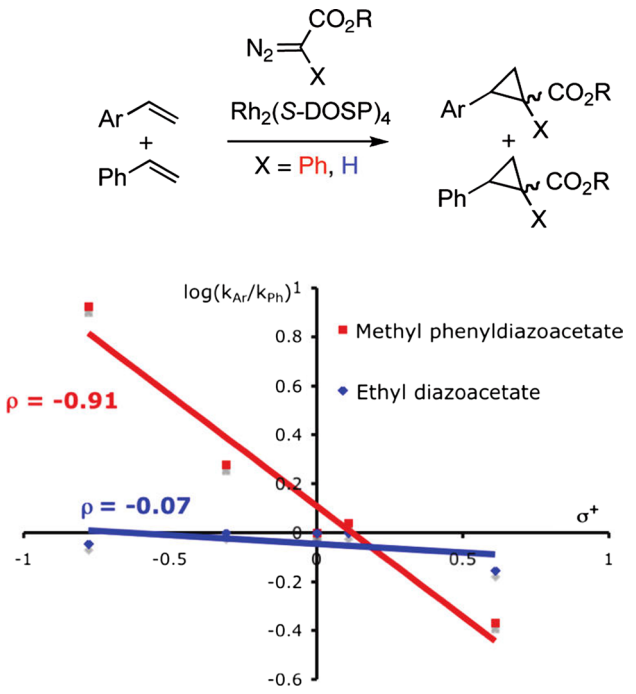

Scheme 1 Competition reaction with styrene. Using metal carbenoids. Reproduced with permission from Ref. [11] Copyright 2000, ScienceDirect

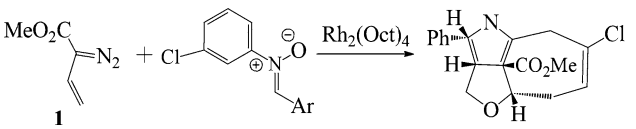

Scheme 2 Dirhodium vinylcarbene-induced nitrone cycloaddition with subsequent cascade carbenoid aromatic cycloaddition/N–O cleavage and rearrangement (CACR)

combined C–H insertion/cope rearrangement [18], and the ylide formation/[2,3]-sigmatropic rearrangement/oxy-cope rearrangement/ene reaction cascade sequence [19]. Furthermore, their propensity for formal [3+2] [20–22] and [4+3] [23–26] cycloaddition reactions has been demonstrated.

Recently, Doyle et al. reported an efficient and highly regioselective cycloaddition reaction between the vinylcarbene from methyl 2-diazo-3-butenoate **1** and diverse nitrones catalyzed by rhodium octanoate [$Rh_2(Oct)_4$] (Scheme 2) [27]. The dirhodium vinylcarbene induced nitrone cycloaddition with subsequent cascade carbenoid aromatic cycloaddition/N–O cleavage, and rearrangement (CACR) gave products which have both oxygen and nitrogen-fused rings and a quaternary carbon in the middle. The compound structure obtained by X-ray diffraction of a single crystal reveals that extensive rearrangement has occurred, and the carboxylate group from the vinyldiazoacetate is bound to the quaternary carbon that connects the tricycle. Even though the reactions were carried out at room temperature, the products of the process were formed with remarkable specificity, and this type of reaction can be used as a general and selective method for preparation of multi-functionalized tricyclic heterocycles through an abnormal cascade process. A further surprising feature of the reactions is that, with *meta*- and *ortho*-substituents on the *N*-aryl group, cyclopropanation could have occurred on either side of the *N*-aryl bond, which would have led to the formation of two regioisomers; however, only a single regioisomer was formed in high yields. Therefore, this multi-step cascade process occurred with very high regiocontrol. This class of reaction has already become a standard method for laboratory and is being considered as a promising protocol for commercial process [28–30].

In light of the experimental results and for further development of the CACR chemistry, it was felt that the deeper understanding of the reaction mechanism, in particular the origins of the observed selectivity on the molecular scale, was indispensable. We report herein the pathways of the rhodium-catalyzed reactions of methyl 2-diazo-3-butenoate and nitrone by using the density functional calculations, which provide the first qualitative account of the experimental data, as well as the structures of important intermediates and transition states involved in the catalytic cycle. The calculations explain how the CACR happens and disclose the reason why the reaction can have such high regioselectivity. It is worthwhile to mention that this is the first report on reaction mechanism for the CACR reaction in detail. The theoretical analysis of the properties of intermediates and transition states revealed unique roles of the rhodium carbene. The studies and mechanistic insights obtained herein can ultimately provide value in accelerating the design and optimization of catalytic processes of transition-metal-catalyzed carbene procedures.

2 Computational methods

2.1 Models

In the present work, we have studied a catalytic model reaction between vinylcarbenoid complex **2** and nitrone **3** to form two different products **4** and **5** using dirhodium tetrakis (formate), $Rh_2(O_2CH)_4$, as a model of a common catalyst [31–34] (Scheme 3). Product **4** is in accord with the actual synthetic compound. The reaction to generating product **5** has not been reported in the literature and was investigated herein for comparison in regioselectivity. These model reactions serve to investigate the fundamental properties of the dirhodium carbene complex, as well as the mechanism and regioselectivity of CACR reactions. The vinylcarbenoid model **2** has been described in previous

Scheme 3 Model reactions for the computational studies

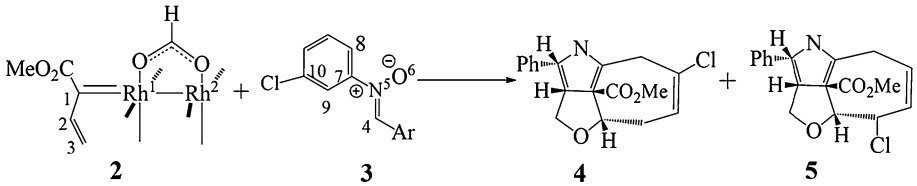

computational studies on cyclopropanation chemistry [31, 34]. This study is focused on an analysis of how the rhodium carbenoid reacts with the nitrone. For detailed discussions on the formation of the reactive vinylcarbenoid complex, see Refs. [31, 34].

2.2 Computational details

All of the calculations were performed with the Gaussian 09 software package [35]. Density functional theory (DFT) was employed using the three-parameter hybrid functional B3LYP [36, 37] to locate stationary points on the potential energy surface (PES). Structures were optimized with a basis set consisting of the 1997 stuttgart relativistic small-core effective core-potential and basis set [Stuttgart RSC 1997 ECP] [38–40] for Rh, augmented with a 4f-function (ζ_f(Rh) = 1.350) [31] and the split valence basis set 6-31G(d,p) for all other atoms (C, H, N, Cl and O). The method and the basis sets used here are known to give reliable results for rhodium (carbene) reactions [5]. This composite basis set is abbreviated 6-31G(d,p)[Rh-RSC+4f]. The main discussion is based on single-point energies calculated at the B3LYP/6-311+G(2d,2p)[Rh-RSC+4f]//B3LYP/6-31G(d,p)[Rh-RSC+4f] level of theory, with zero-point energy corrections calculated at the B3LYP/6-31G(d,p)[Rh-RSC+4f] level and Gibbs free energies calculated at the B3LYP/6-31G(d,p)[Rh-RSC+4f] level of theory. Heavy-atom basis set definitions and corresponding pseudopotential parameters were obtained from the EMSL basis set exchange library [41, 42]. Each stationary point was adequately characterized by normal coordinate analysis (only one imaginary for a transition state and no imaginary frequencies for an equilibrium structure). The intrinsic reaction coordinate (IRC) analysis [43] was carried out throughout the reaction pathways to confirm that all stationary points are smoothly connected to each other.

To evaluate the effect of the solvent polarity on the energetics of CACR reactions, a single-point energy calculation was performed with self-consistent reaction field (SCRF) method [based on the SMD model [44], ε = 10.125 for dichloroethane (DCE)]. Natural population analysis and natural bond orbital (NBO) analyses were carried out at the same level as the one used for geometry optimization [45, 46]. All charge distribution analyses discussed throughout this article are made on the basis of the nature population analysis.

3 Results and discussion

3.1 Reaction to produce the real product 4

First, we investigated the reactions of **3** with vinylcarbenoid complex **2** to generate product **4** as a basic model reaction. Scheme 4 shows the reaction course that the catalytic cycle involves five steps. The free energy profile of this CACR reaction in the gas phase is given in Fig. 1. First, **3** and **2** interact through a stepwise [3+2] cycloaddition to form the complex **III**. The formation of C–O bond proceeds via **TSI** with an activation free energy of 2.8 kcal/mol, which is followed by the formation of C–C bond with the activation free energy barrier of 4.5 kcal/mol. Subsequent intramolecular cyclopropanation by the rhodium carbene on the nitrogen-bound aryl group is proposed to form intermediate **V** via two transition states **TSIII** and **TSIV** with the free energy barriers of 10.2 and 7.6 kcal/mol, respectively, and the catalyst is regenerated. The next step toward the final product first involves an electrocyclic opening of the cyclopropane ring (aromatic cycloaddition) to form intermediate **VI** via **TSV** with a free energy barrier 4.5 kcal/mol. Unexpected and unique N–O bond cleavage and [1,7]-oxygen migration then take place through **TSVI** with the largest free energy barrier of 22.2 kcal/mol followed by a downhill path to the final product with large exothermicity (64.7 kcal/mol). In **TSVI**, the cleavage of N–O bond and migration of oxygen to conjugated olefinic carbon atom take place simultaneously in a single step. No intermediates were located near **TSVI** along the intrinsic reaction coordinate.

To probe the solvent effect on the reaction energetics, SCRF calculations (SMD model) were performed based on the gas-phase geometry. Dichloroethane (DCE, ε = 10.125) was investigated as the solvent because it is used for the CACR reaction in practice. The relative free energies of the stationary points on the potential energy surface in DCE are also given in Fig. 1 (in blue). The free energy profile did not change very much from the one in the gas-phase calculations. The N–O cleavage and [1,7]-oxygen migration processes have the largest free energy barrier (19.6 kcal/mol in DCE). Therefore, this step can be regarded as the rate-determining step (RDS). Moreover, the free energy barrier for **TSVI** has a small decrease, and the energy barrier for cyclopropanation has a slight increase. As compared to the free energy profile in gas phase, the [1,7]-oxygen migration

Scheme 4 Pathway of the $Rh_2(O_2CH)_4$-catalyzed CACR reaction of **2** and **3** to produce **4**

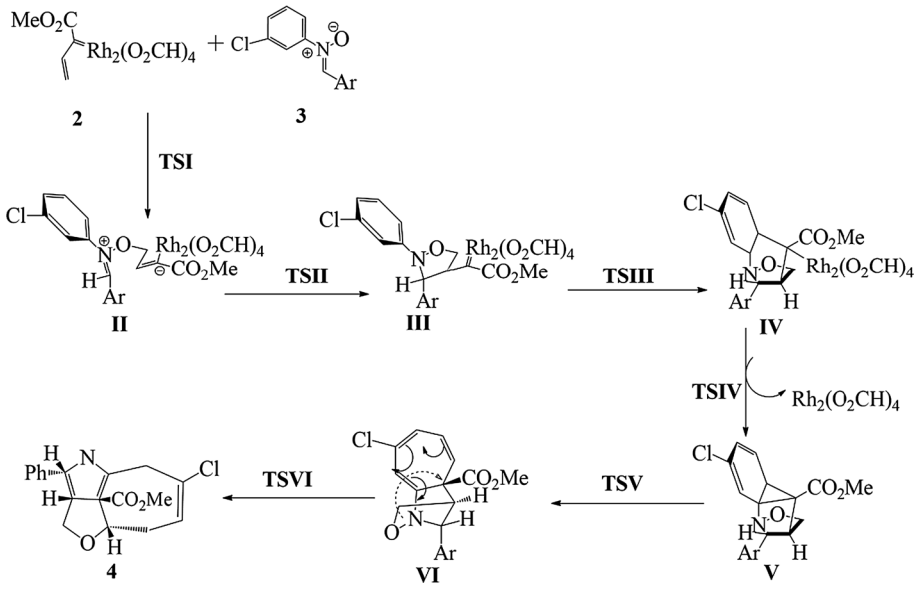

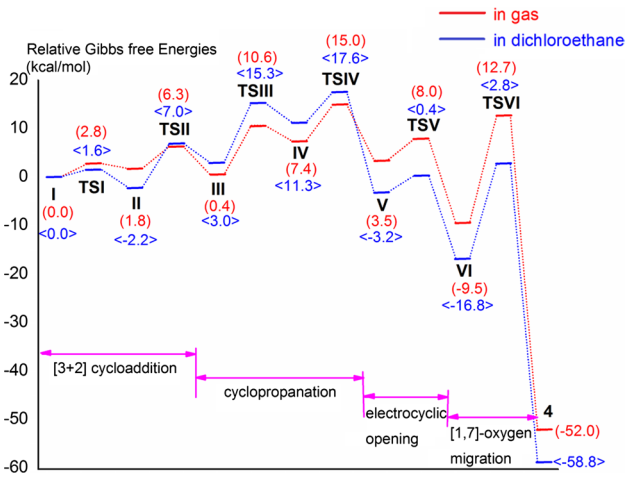

Fig. 1 Free energy profile of the $Rh_2(O_2CH)_4$-catalyzed CACR reaction of **2** and **3** to produce **4** at the B3LYP/6-311+G(2d,2p)[Rh-RSC+4f]//B3LYP/6-31G(d,p)[Rh-RSC+4f] level. The result of the free energies in gas phase is given in *red*, and the result of the free energies in DCE is shown in *blue*

step has the highest energy barrier, which suggests that how to overcome the energetic bottleneck for the [1,7]-oxygen migration becomes very crucial for accelerating the reaction rate.

The 3D structures of representative stationary points are shown in Fig. 2. The Rh^1–Rh^2 bond of **I** has no significant change toward the formation of the complex **III** (2.479 → 2.474 Å). The Rh^1–C^1 bond of **I** (2.036 Å) has a significant increase in first to form the intermediate **II** (2.103 Å) and then shortens through the C–C bond formation stage **TSII** (2.063 Å) to form the complex **III** (1.981 Å, 5.8 % decrease), which indicates that **II** barely has the character of carbene complex. To probe the function of the nuclear structure of the dirhodium catalyst, we analyzed the nature of the Rh–Rh–C π and σ-bond systems in **II** (carbene complex). Important orbital of **II** is shown in Fig. 3. LUMO of the complex **II** was found to be exactly what is expected and composed mainly of the carbene 2p orbital, which accepts rather small back-donation form the Rh^1 $4d_{xz}$ orbital to form an extended π*-system that possesses a strongly electrophilic carbene carbon.

Analysis of the charge distribution during the reaction course was found to be informative and showed strong parallelism between this realistic model to form **4** (Fig. 4a), and the model to form **5** discussed later (Fig. 4b). The nitrone moiety releases negative charge (C^4: +0.03 → +0.16, O^6: −0.51 → −0.42) upon formation of **II**, and the negative charge moves largely into the vinylcarbene carbon C^1 (+0.04 → −0.12) and the N^5 atom (+0.09 → +0.01). In the C^2–C^4 bond formation stage (**TSII**), the nitrogen moiety becomes less positive (N^5: +0.01 → −0.15, C^4: +0.16 → −0.06), and the carbene carbon becomes cationic (−0.12 → +0.16).In the complex **IV**, the benzene ring attached to N^5 atom significantly becomes more positive (C^7: +0.15 → +0.31), because the negative charge moves largely from the p-type orbital of the C^7 into the C^1 atom. The Charge of the Rh^1 and Rh^2 atoms changes just a little during the C^1–C^8 bond formation (Rh^1: +0.44 → +0.47; Rh^2: +0.51 → +0.55).However, in the C^1–C^7 bond formation, Rh^1 and Rh^2 lose a lot of negative charge (Rh^1: +0.47 → +0.68; Rh^2: +0.55 → +0.68) and C^7 becomes less positive (+0.31 → +0.13), which is in accord with the removing of the donation from carbene to Rh. In the electrocyclic reaction TS (**TSV**), the C^1–C^7 and C^1–C^8 bond significantly shorten (1.580–1.503 and 1.537–1.490 Å, respectively.), and C^7 and C^8 atom lose negative charge (C^7: +0.13 → +0.20, C^8: −0.26 → −0.19). The negative

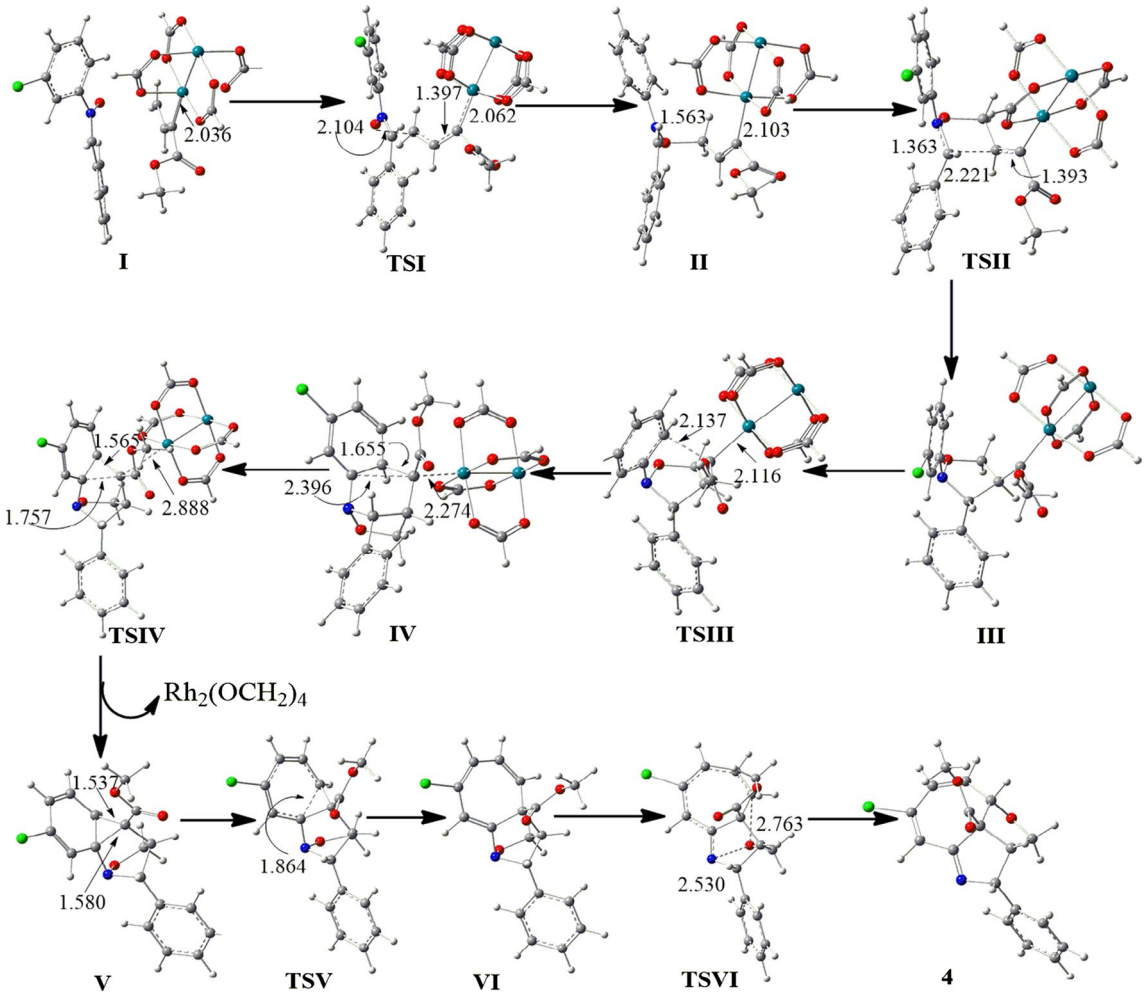

Fig. 2 B3LYP/6-31G(d,p)[Rh-RSC+4f] structures of stationary points in CACR reaction of **2** and **3**–**4**. The *numbers* refer to bond length (Å)

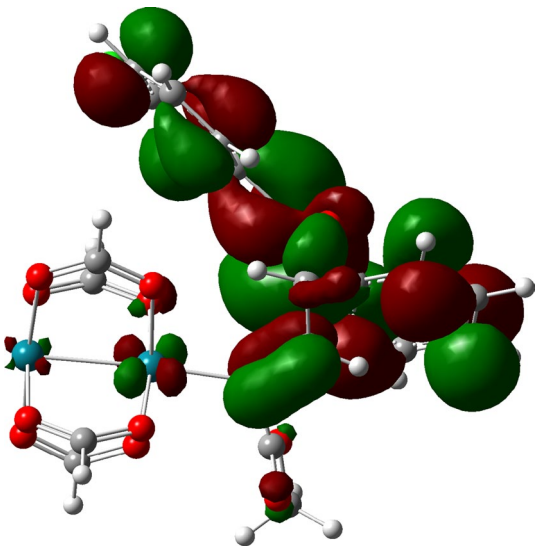

Fig. 3 Electronic structure and shape of the frontier electronic level (LUMO) of complex **II**

charge moves largely into the C^1 atom (−0.16 → −0.22). In [1,7]-oxygen migration step, the C^7–N^5 bond shortens (1.449 Å → 1.282 Å), and the benzene ring attached to N^5 loses negative charge (C^7: +0.20 → +0.25, C^8: −0.19 → +0.06). The nitrone moiety becomes negatively charged (N^5 decrease by +0.21) because of forming of the C^7–N^5 π-bonding electrons. Some negative charge is also transferred to the O^6 atom (−0.13).

3.2 Reaction to produce isomer **5**

Furthermore, to prove the reasonableness of the mechanism proposed for the above catalytic system and gain insight into the influencing factors for highly regioselectivity for the present reaction, the other reaction of nitrone **3** with dirhodium vinylcarbene **2** to produce **5** was investigated. The free energy profile along the reaction progress is shown in Fig. 5. To make a concise expression, the detailed reaction mechanism to form **5** is shown in Fig. 6.

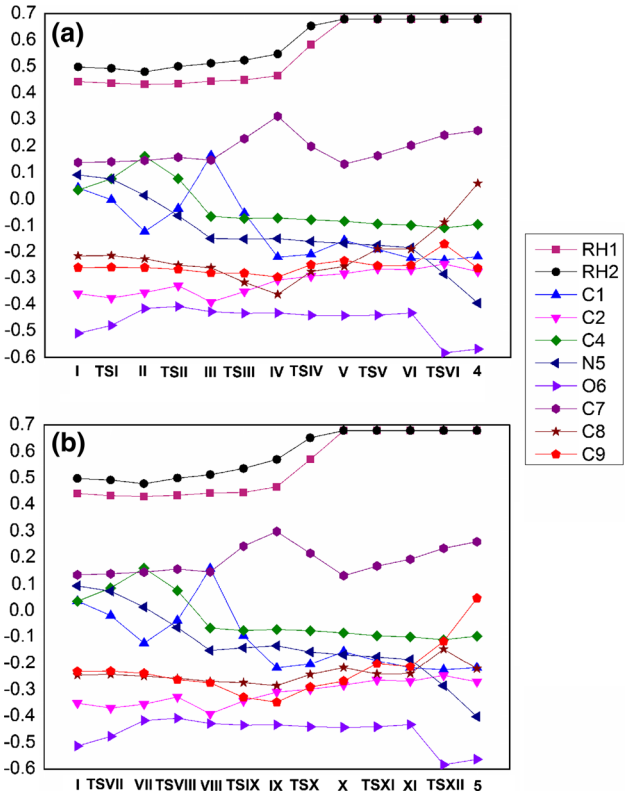

Fig. 4 Charge distribution along the reaction coordinate for **a** the reaction to **4** and **b** the reaction to **5**

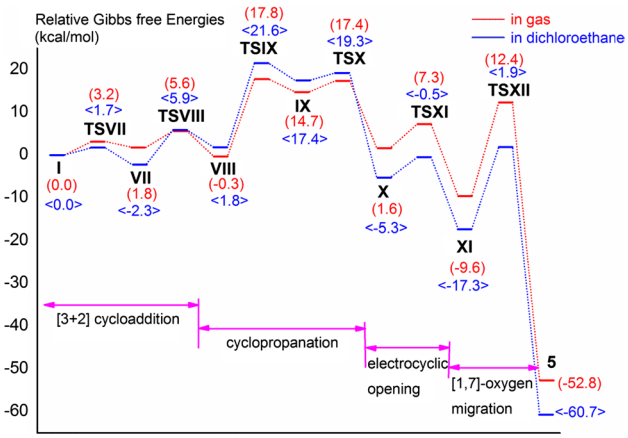

Fig. 5 Free energy profile of the $Rh_2(O_2CH)_4$-catalyzed CACR reaction of **2** and **3** to produce **5** at the B3LYP/6-311+G(2d,2p)[Rh-RSC+4f]//B3LYP/6-31G(d,p)[Rh-RSC+4f] level. The result of the free energies in gas phase is given in *red*, and the result of the free energies in DCE is shown in *blue*

The reaction pathway and the energetics obtained for this reaction are essentially the same as those of the reaction to form **4** (Fig. 1). The CACR reaction also starts with the [3+2]-cycloaddition. This step goes through stepwise mechanism via **TSVII** and **TSVIII** with low free energy barriers of 3.2 and 3.8 kcal/mol, respectively, in the gas phase. The charge distribution shows the same tendency as found for the reaction to form **4**. In the next cyclopropanation step, carbene atom C^1 reacts with C^9 instead of C^8 to form the intermediate **IX**. Unlike the result in the reaction to obtain **4**, the C^1–C^9 bond formation step process via transition state **TSIX** with a significantly higher activation free energy (18.1 kcal/mol in gas phase). In the next electrocyclic opening of the cyclopropane ring, the free energy barrier for overcoming **TSXI** is much lower ($\Delta G^{\neq} = 5.7$ kca/mol). Downhill from **TSXI**, seven-membered ring intermediate **XI** is formed. Since the activation of the N–O bond is poor, the electrophile attack of O to C^9 via a concerted transition state **TSXII** requires a higher Gibbs free energy of activation of 22.0 kcal/mol in gas phase, which is nearly identical with that of the reaction to form **4** (22.2 kcal/mol). When taking the solvent effect into consideration, the energy profile has a little different from that in gas phase. The step of [1,7]-oxygen migration also bears a large free energy barrier (19.2 kcal/mol), which indicates that the oxygen migration is also difficulty in all cases. However, in the reaction to form **5**, the C^1–C^9 bond formation bears the largest energy barrier (19.8 kcal/mol) and the cyclopropanation step has become the rate-determining step (RDS).

Two reactions mentioned above affording **4** and **5** are two parallel. Based on our calculational results, although the free energy barrier of RDS to **5** is larger than that to **4**, the difference between those two reactions is small. So the reaction dynamics is not the main factor responsive to the fact that the amount of product **4** dominates over **5** in DCE. We noted that an acidic additive 1,1,1,3,3,3-hexafluoro-2-propanol (HFIP) was used to capture the basic product in the experiment research [27]. So the proportion of alkaline dissociation equilibrium constant K_b values of products **4** and **5** was also calculated in our study according to the Eqs. (1) and (2).

$$\mathrm{B} + \mathrm{H}^+ \overset{\Delta G_B^{\theta}}{\rightleftharpoons} \mathrm{BH}^+ \tag{1}$$

$$\frac{K_{b,4}}{K_{b,5}} = \exp\left(-\frac{\Delta G_4^{\theta} - \Delta G_5^{\theta}}{RT}\right) = \exp\left(\frac{G_4^{\theta} - G_{\mathrm{H4}^+}^{\theta} - G_5^{\theta} + G_{\mathrm{H5}^+}^{\theta}}{RT}\right) \tag{2}$$

where ΔG_4^{θ} and ΔG_5^{θ} are the free energy changes of reactions corresponding to producing **4** and **5** in the standard state, respectively. R is mole gas constant, and T equals to 298.15 K. Table 1 lists the Gibbs free energies of product **4** and **5**, as well as their corresponding protonated substances $\mathbf{H4}^+$ and $\mathbf{H5}^+$. It is easy to find that the basicity of the product **4** is stronger than that of the product **5**. As a

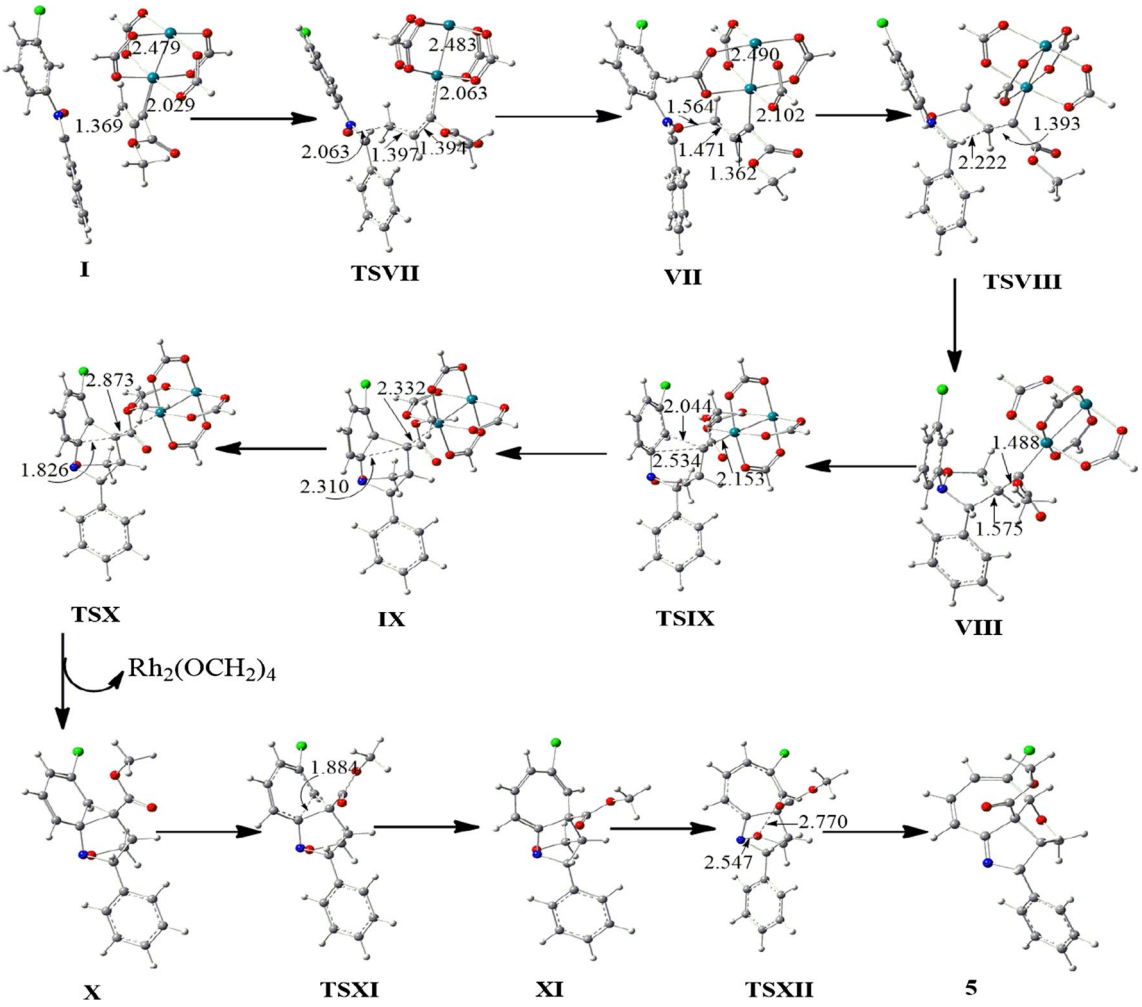

Fig. 6 B3LYP/6-31G(d,p)[Rh-RSC+4f] structures of stationary points in CACR reaction of **2** and **3**–**5**. The *numbers* refer to bond length (Å)

Table 1 Gibbs free energy (in kcal/mol) of product **4** and **5**, and their corresponding protonated substances **H4**$^+$ and **H5**$^+$ in DCE

Substance **B**	**4**	**H4**$^+$	**5**	**H5**$^+$
G_B^{θ}/kcal mol^{-1}	−1,435.3	−1,437.0	−1,437.2	−1,438.1

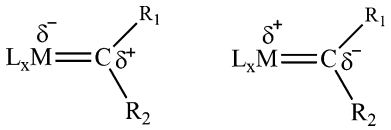

Fig. 7 Fischer and Schrock-type carbenoids

result, HFIP more easily reacts with **4** than **5**, and thus, the reaction equilibrium will move to the formation of product **4**, which is consistent with the experimental results that the reaction between **1** and **3** has high regioselectivity.

It is well known that rhodium carbenoids are Fischer-type carbenoids (see Fig. 7). From the charge distribution along the reactions, it is clear that the carbene C^1 atom occurs electrophilic addition, along with a significant reduction of its charge. When there is an electron-withdrawing group such as chlorine at C^{10} of nitrone,the charge density of chlorine's *ortho*-site decreases due to the negative inductive effect of chlorine. On the other hand, the electron density on C^8 is slightly affected by the negative inductive effect of chlorine. Therefore, the electrophilic addition is more likely to occur at C^8 site, rather than C^9 site.

4 Conclusion

On the basis of our theoretical computations, we have developed a mechanistic proposal for the CACR reaction. The present studies have revealed, for the first time, the

energetics, the electronic nature, and the 3-D structures of the intermediates and the transition states in the catalytic cycle of the dirhodium vinylcarbene-induced nitrone cycloaddition with subsequent cascade carbenoid aromatic cycloaddition/N–O cleavage and rearrangement. The reaction of vinyldiazoacetate-induced nitrone starts from the stepwise [3+2] cycloaddition. Subsequent intramolecular cyclopropanation and electrocyclic opening of the cyclopropane ring by the rhodium carbene on the nitrogen-bound aryl group take place to form a heptatomic ring intermediate. A [1,7]-oxygen migration to final product occurs via a concerted transition state. The reactions to form **4** and **5** have similar mechanisms, and the step of cyclopropanation is the regioselectivity determining step. With *meta*-substituent (Cl) on the *N*-aryl group, the charge density of chlorine's *ortho*-site decreases due to the negative inductive effect of chlorine. Therefore, as compared to the electrophilic addition on the C^8 atom, the electrophilic addition on the C^9 site owns a significantly incensement on the energy barrier of cyclopropane (**TSIII** and **TSIX**). Since the basicity of the product **4** is stronger than that of the product **5**, the acidic additive HFIP promotes the formation of product **4**.

5 Supporting information

The optimized Cartesian coordinates and geometrical structures of all stationary points along the potential energy profiles. This material is available free of charge via the Internet at http://springerlink.lib.tsinghua.edu.cn/content/.

Acknowledgments This project has been supported by the National Natural Science Foundation of China (Grant No. 21173151) and by National Basic Research Program of China of Ministry of Science and Technology of China (973 Program, Grant No. 2011CB201202).

References

1. Selander N, Fokin VV (2012) J Am Chem Soc 134:2477–2480
2. Nadeau E, Ventura DL, Brekan JA, Davies HML (2010) J Org Chem 75:1927–1939
3. Cui X, Xu X, Lu H, Zhu S, Wojtas L, Zhang XP (2011) J Am Chem Soc 133:3304–3307
4. Takeda K, Oohara T, Shimada N, Nambu H, Hashimoto S (2011) Chem Eur J 17:13992–13998
5. Hansen JH, Gregg TM, Ovalles SR, Lian Y, Autschbach J, Davies HML (2011) J Am Chem Soc 133:5076–5085
6. Doyle MP, McKervey MA, Ye T (1998) Modern catalytic methods for organic synthesis with diazo compounds. Wiley, London
7. Davies HML, Antoulinakis EG (2004) Intermolecular metal-catalyzed carbenoid cyclopropanations. In: Organic reactions, vol 57. Wiley, USA
8. Davies HM, Beckwith RE (2003) Chem Rev 103:2861–2904
9. Davies HM, Loe O, Budynina E, Averina E, Ivanova O, Yashin N, Kuznetsova T, Zefirov N, VanZanten A, Mullaugh K (2004) Synthesis 2004:2595–2608
10. Davies HM, Manning JR (2008) Nature 451:417–424
11. Davies HM, Panaro SA (2000) Tetrahedron 56:4871–4880
12. Qin C, Boyarskikh V, Hansen JH, Hardcastle KI, Musaev DG, Davies HML (2011) J Am Chem Soc 133:19198–19204
13. Davies HM, Morton D (2011) Chem Soc Rev 40:1857–1869
14. Lu H, Dzik WI, Xu X, Wojtas L, de Bruin B, Zhang XP (2011) J Am Chem Soc 133:8518–8521
15. Lian Y, Davies HML (2011) J Am Chem Soc 133:11940–11943
16. Davies HM, Denton JR (2009) Chem Soc Rev 38:3061–3071
17. Doyle MP, Duffy R, Ratnikov M, Zhou L (2009) Chem Rev 110:704–724
18. Davies HML, Stafford DG, Doan BD, Houser JH (1998) J Am Chem Soc 120:3326–3331
19. Parr BT, Li Z, Davies HM (2011) Chem Sci 2:2378–2382
20. Barluenga J, Lonzi G, Riesgo L, López LA, Tomás M (2010) J Am Chem Soc 132:13200–13202
21. Lian Y, Davies HML (2009) J Am Chem Soc 132:440–441
22. Davies HML, Xiang B, Kong N, Stafford DG (2001) J Am Chem Soc 123:7461–7462
23. Reddy RP, Davies HML (2007) J Am Chem Soc 129:10312–10313
24. Schwartz BD, Denton JR, Lian Y, Davies HML, Williams CM (2009) J Am Chem Soc 131:8329–8332
25. Lian Y, Miller LC, Born S, Sarpong R, Davies HML (2010) J Am Chem Soc 132:12422–12425
26. Miller LC, Ndungu JM, Sarpong R (2009) Angew Chem Int Ed 48:2398–2402
27. Wang X, Abrahams QM, Zavalij PY, Doyle MP (2012) Angew Chem Int Ed 51:5907–5910
28. Tabolin AA, Ioffe SL (2014) Chem Rev 114. doi:10.1021/cr400196x
29. Xu X, Doyle MP (2014) Acc Chem Res 47:1396–1405
30. Xu X, Leszczynski JS, Mason SM, Zavalij PY, Doyle MP (2014) Chem Commun 50:2462–2464
31. Hansen J, Autschbach J, Davies HML (2009) J Org Chem 74:6555–6563
32. Nakamura E, Yoshikai N, Yamanaka M (2002) J Am Chem Soc 124:7181–7192
33. Yoshikai N, Nakamura E (2003) Adv Synth Catal 345:1159–1171
34. Nowlan DT, Gregg TM, Davies HML, Singleton DA (2003) J Am Chem Soc 125:15902–15911
35. Frisch MJGWT, Schlegel HB, Scuseria GE, Robb MA, Cheeseman JR, Scalmani G, Barone V, Mennucci B, Petersson GA, Nakatsuji H, Caricato M, Li X, Hratchian HP, Izmaylov AF, Bloino J, Zheng G, Sonnenberg JL, Hada M, Ehara M, Toyota K, Fukuda R, Hasegawa J, Ishida M, Nakajima T, Honda Y, Kitao O, Nakai H, Vreven T, Montgomery JA Jr, Peralta JE, Ogliaro F, Bearpark M, Heyd JJ, Brothers E, Kudin KN, Staroverov VN, Kobayashi R, Normand J, Raghavachari K, Rendell A, Burant JC, Iyengar SS, Tomasi J, Cossi M, Rega N, Millam JM, Klene M, Knox JE, Cross JB, Bakken V, Adamo C, Jaramillo J, Gomperts R, Stratmann RE, Yazyev O, Austin AJ, Cammi R, Pomelli C, Ochterski JW, Martin RL, Morokuma K, Zakrzewski VG, Voth GA, Salvador P, Dannenberg JJ, Dapprich S, Daniels AD, Farkas O, Foresman JB, Ortiz JV, Cioslowski J, Fox DJ (2009) Gaussian 09, revision A.1. Gaussian Inc, Wallingford, CT
36. Becke AD (1993) J Chem Phys 98:5648–5652
37. Lee C, Yang W, Parr RG (1988) Phys Rev B 37:785–789
38. Kaupp M, Schleyer PVR, Stoll H, Preuss H (1991) J Chem Phys 94:1360–1366
39. Bergner A, Dolg M, Küchle W, Stoll H, Preuß H (1993) Mol Phys 80:1431–1441
40. Dolg M, Stoll H, Preuss H, Pitzer RM (1993) J Phys Chem 97:5852–5859
41. Feller D (1996) J Comput Chem 17:1571–1586

42. Schuchardt KL, Didier BT, Elsethagen T, Sun L, Gurumoorthi V, Chase J, Li J, Windus TL (2007) J Chem Inf Model 47:1045–1052
43. Foresman JB, Keith TA, Wiberg KB, Snoonian J, Frisch MJ (1996) J Phys Chem 100:16098–16104
44. Marenich AV, Cramer CJ, Truhlar DG (2009) J Phys Chem B 113:6378–6396
45. Reed AE, Curtiss LA, Weinhold F (1988) Chem Rev 88:899–926
46. Yang X, Fan L, Xue Y (2014) RSC Adv 4:30108–30117